Inorganic Chemistry

Article

pubs.acs.org/IC

Uranyl Sensitization of Samarium(III) Luminescence in a Two-Dimensional Coordination Polymer

Karah E. Knope,[†] Daniel T. de Lill,[‡] Clare E. Rowland,[†] Paula M. Cantos,[†] Ana de Bettencourt-Dias,*[,‡] and Christopher L. Cahill*[,†]

[†]Department of Chemistry, The George Washington University, 725 21st Street NW, Washington, D.C. 20052, United States

[‡]Department of Chemistry, The University of Nevada, Reno, 1664 North Virginia Street, Reno, Nevada 89557, United States

Supporting Information

ABSTRACT: Heterometallic carboxyphosphonates UO_2^{2+}/Ln^{3+} have been prepared from the hydrothermal reaction of uranyl nitrate, lanthanide nitrate (Ln = Sm, Tb, Er, Yb), and phosphonoacetic acid (H_3PPA). Compound **1**, $(UO_2)_2(PPA)(HPPA)_2Sm(H_2O)\cdot 2H_2O$ (**1**) adopts a two-dimensional structure in which the UO_2^{2+} metal ions bind exclusively to the phosphonate moiety, whereas the Ln^{3+} ions are coordinated by both phosphonate and carboxylate functionalities. Luminescence studies of **1** show very bright visible and near-IR samarium(III)-centered emission upon direct excitation of the uranyl moiety. The Sm^{3+} emissive state exhibits a double-exponential decay with lifetimes of 67.2 ± 6.5 and 9.0 ± 1.3 μs as measured at 594 nm, after excitation at both 365 and 420 nm. No emission is observed in the region typical of the uranyl cation, indicating that all energy is either transferred to the Sm^{3+} center or lost to nonradiative processes. Herein we report the synthesis, crystal structure, and luminescent behavior of **1**, as well as those of the isostructural terbium, erbium, and ytterbium analogues.

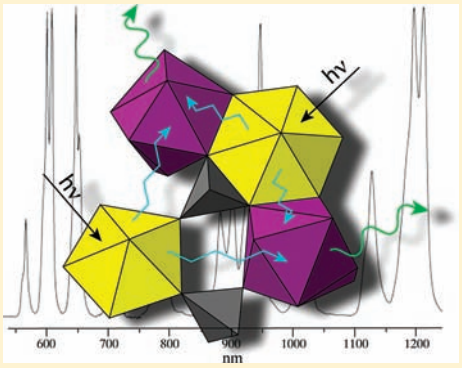

INTRODUCTION

As the field of hybrid materials, including metal−organic frameworks (MOFs) and coordination polymers (CPs), matures, its influence is felt further and further out in the periodic table. By now, it has encountered the actinides, and among them it has found particular favor with uranium. In addition to the usual (i.e., utilitarian) reasons for studying MOFs, uranium-containing hybrid materials are interesting for historically and politically founded reasons. Both weapons legacy waste from the last century and the environmental implications of the nuclear fuel cycle have made the interaction of uranium with environmentally (biologically and geologically) relevant functional groups particularly meaningful.[1−3] Among the more pertinent functional groups in environmental systems are carboxylates and phosphonates, both of which have been successfully employed in the synthesis of uranium-containing hybrid materials.[4−10] For example, the use of carboxyphosphonates as ligands permits both functionalities to be incorporated into a single compound.[11−15] The presence of a heterofunctional ligand opens up a second possibility, namely the introduction of a second metal center. In fact, the affinity of the harder metal for the harder functionality (and vice versa) has been exploited to create heterometallic UO_2^{2+}-TM^{2+} compounds.[4,16−20]

Reports of heterometallic uranyl-lanthanide hybrid compounds, by comparison, are fairly rare in the literature,[21−24] and most, if not all, have been constructed using carboxylate-functionalized organic ligands. Yet within separations chemistry, reactions of lanthanide and actinide metal cations with phosphonate chelating agents have received considerable attention because of their unusually high stability.[25−28] Both lanthanide and actinide cations are known to form strong complexes with phosphonate donor ligands whose relative stabilities are orders of magnitude greater than those of carboxylate ligands with comparable acidity.[26,27] For a given ligand, separations schemes often rely on small differences in the stability of lanthanide and actinide complexes for successful separation. Using this idea, in this work, we aimed to capitalize on differences in the affinity of the UO_2^{2+} versus Ln^{3+} ions for phosphonate and carboxylate moieties as well as steric restraints imposed by very different coordination geometries of the metal ions to prepare UO_2^{2+}/Ln^{3+} heterometallic materials. Further, can luminescence of the uranyl cation be used to stimulate lanthanide emission?

Lanthanide luminescence results from f−f transitions, which possess low molar absorptivities, leading to inefficient direct excitation of the ion.[29,30] As such, it is common to sensitize lanthanide emission through a donor, typically an organic ligand. In this process, commonly referred to as the antenna effect, the donor is excited and, subsequently, transfers energy to the lanthanide ion, which can then decay through luminescence. To be effective, it is necessary for the energy levels of the donor to be near enough to the acceptor to allow energy transfer to occur but not too close to allow loss of energy via back-transfer to the donor or other energy migration pathways.

Received: July 8, 2011
Published: December 15, 2011

   dx.doi.org/10.1021/ic201450e | *Inorg. Chem.* 2012, 51, 201−206

For europium(III) and terbium(III) systems, it has been found that the emissive level should be roughly 2500−5000 cm^{-1} below the donating energy level for efficient sensitization to occur.[31] The optimum energy gap has not been empirically determined for other lanthanide complexes, most likely due to the increasing capacity of other lanthanide ions to lose their energy to nonradiative processes arising from smaller energy gaps between the emissive and ground states. However, the $^6G_{5/2}$ emissive excited state of samarium(III) at 17 800 cm^{-1} is close to the europium(III) $^5D_0$ emissive level at 17 300 cm^{-1}, leading thus to the assumption that the emissive state of UO_2^{2+}, situated close to 20 000 cm^{-1}, may be appropriately positioned to sensitize samarium(III) emission. While uranyl sensitization of Eu^{3+} has been relatively well studied,[32−37] there are few reports of using Sm^{3+} in a similar fashion, and these are primarily in oxide lattices rather than in CPs, as seen here.[38−44] While synthesis of the europium analogue of the title compound was not successful, the samarium compound provides a suitable alternative model system to explore this assumption.

The ability to predictably select a second metal using the heterofunctional carboxyphosphonate ligand phosphonoacetic acid (H_3PPA) and the promise of uranyl-sensitized lanthanide emission prompted the hydrothermal synthesis of $(UO_2)_2(PPA)(HPPA)_2Sm(H_2O)\cdot 2H_2O$ (**1**), as well as isostructural erbium, terbium, and ytterbium analogues. In addition to the crystal structure, we present luminescence data confirming uranyl sensitization of samarium. The luminescent behavior of the terbium and erbium analogues is also discussed. These lanthanide ions offer the opportunity to explore uranyl sensitization of lanthanide emission within inorganic−organic hybrid systems, with lanthanide emitting levels lying above, just below, and well below the emissive level of the uranyl cation, respectively.

EXPERIMENTAL SECTION

Synthesis. ***Caution!*** *Whereas the uranium oxynitrate hexahydrate, $(UO_2)(NO_3)_2\cdot 6H_2O$, used in this investigation contains depleted uranium, standard precautions for handling radioactive substances should be followed.*

Compound **1** was synthesized hydrothermally. Uranium oxynitrate hexahydrate (0.177 g, 0.35 mmol), phosphonoacetic acid, 98% (0.098 g, 0.67 mmol), samarium nitrate hexahydrate (0.169 g, 0.38 mmol), 5 M ammonium hydroxide (0.150 mL, 3.7 mmol), and distilled water (4 g, 278 mmol) were combined in a 23 mL Teflon-lined Parr bomb in an approximate molar ratio of 1:2:1:10:794, respectively, to give a solution of pH 1.6. The reaction vessel was then sealed and heated statically at 150 °C for 3 days. Upon cooling to room temperature, a clear yellow solution (pH 1.5) was decanted and yellow platelike crystals were obtained. The crystals were washed with water, sonicated in ethanol, washed with ethanol, and then allowed to air-dry at room temperature (yield 35% based on uranium). Elemental analysis was performed by Galbraith Laboratories (Knoxville, TN). Obsd (calcd) for samarium: C, 5.90 (6.23); H, 1.10 (1.22). Obsd (calcd) for erbium: C, 6.14 (6.14); H, 1.05 (1.20). Isostructural terbium, erbium, and ytterbium analogues of compound **1** were prepared by replacing samarium nitrate with the corresponding lanthanide nitrate salt, and structures were confirmed via powder X-ray diffraction (XRD; Figure S1 in the Supporting Information).

X-ray Structure Determination. A single crystal was isolated from the product and mounted on a Micromount needle (MiTeGen). Reflections were collected at 100 K on a Bruker SMART diffractometer equipped with an APEX II CCD detector using Mo Kα radiation and a combination of 0.5° ω and φ scans. Details of the data collection and refinement can be found in Table 1. The data were integrated and corrected for absorption using the *APEX2* suite of crystallographic software.[45] The structure was solved using direct methods and refined using *SHELXL-97*[46] within the *WinGX* software suite.[47] A search for higher symmetry using *PLATON*[48] suggested no changes to the space group. Hydrogen atoms could be located in the Fourier electron difference map but could not be satisfactorily refined and were therefore placed in calculated positions.

Table 1. Crystallographic Structure Refinement Data for 1

empirical formula	$C_6H_{14}O_{22}P_3SmU_2$
fw	1157.49
temperature (K)	100
λ(Mo Kα)	0.7103
cryst syst	monoclinic
space group	$P2_1/c$
a (Å)	10.9448(15)
b (Å)	10.2738(14)
c (Å)	20.392(3)
β (deg)	103.451(2)
V (Å)	2230.1(5)
Z	4
D_{calc} (g/cm^3)	3.448
μ (mm^{-1})	17.403
GOF on F^2	1.058
R1[a] [$I > 2\sigma(I)$]	0.0403
wR2[a]	0.0846

[a] $R1 = \sum||F_o| - |F_c||/\sum|F_o|$; $wR2 = \{\sum[w(F_o^2 - F_c^2)^2/\sum[w(F_o^2)^2]\}^{1/2}$.

Positional disorder of one of three crystallographically unique PPA ligands over two positions required using a PART command, wherein the dominant component (A) accounted for 78% of the PPA ligand. The total occupancy of the major (A) and minor (B) components was fixed to 100%, with B therefore accounting for 22%. A SAME command was used to ensure that the two components were modeled similarly. Disagreeable thermal parameters in component B required the use of an EADP command to fix thermal parameters to match those of similar atoms in component A (i.e., C5B was fixed to the values of C5A). Crystallographic data may also be obtained free of charge from the Cambridge Crystallographic Data Centre (CCDC) at http://www.ccdc.cam.ac.uk/ by referencing CCDC 777417.

Powder XRD data were collected using a Rigaku Miniflex diffractometer (Cu Kα, 3−60°). The observed and calculated patterns were compared to confirm that the single crystal was representative of the bulk and both were in agreement. Powder XRD was additionally used to confirm that phases synthesized using other lanthanides were isostructural with **1**. Note that the ytterbium analogue could not be prepared as a pure phase. Powder XRD data are available as Supporting Information (Figure S1).

Luminescence. Luminescence and lifetime measurements were conducted on a powdered sample using a Horiba Jobin Yvon Spex Fluorolog-3 fluorimeter. The sample was placed into the solid-state sample holder with a quartz cover window and was excited at 45° with a 450 W continuous-wave xenon lamp through a double-grating excitation monochromator with 1200 grooves/mm and blazed at 330 nm. Emission detection was done at 45° through a double-grating emission monochromator [1200 grooves/mm for visible and 600 grooves/mm for near-IR (IR)] with a 500 nm blaze. Samples were excited at 365 and 420 nm, and a diffuse-reflectance spectrum can be found in Figure S2 in the Supporting Information. These are charge-transfer bands, well-known to result in emission from uranyl centers, and are nominally $3\sigma_u \rightarrow 5f_\delta$ and $3\sigma_u \rightarrow 5f_\phi$ transitions (~420 nm) and charge transfer from equatorial ligands (~365 nm). This is an admittedly simplistic description of these transitions yet suffices for the purpose of the experiments (and results) described herein. Further details of these transitions may be found in an extensive treatment by Denning.[49]

Visible emission was detected using a R928P photomultiplier tube (emission/excitation slits at 5 nm), whereas NIR emission (emission/excitation slits at 1 nm) was detected with a liquid-nitrogen-cooled Hamamatsu R5509-73 near-IR photomultiplier tube. Lifetime

dx.doi.org/10.1021/ic201450e | Inorg. Chem. 2012, 51, 201−206

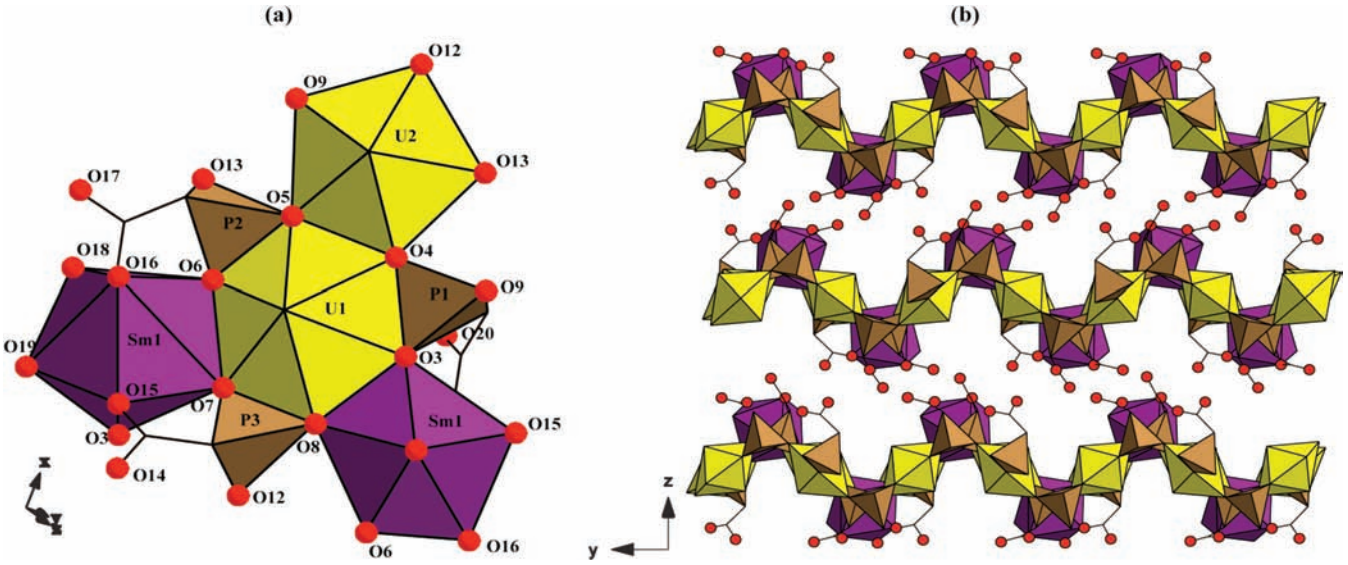

Figure 1. Polyhedral representation of (a) the local structure of **1** and (b) the packing diagram of **1** viewed down the [100] direction. Yellow polyhedra represent U^{VI} atoms in hexagonal- and pentagonal-bipyramid geometries. Purple polyhedra are eight-coordinate Sm^{3+} sites. Brown polyhedra, black lines, and red circles represent phosphorus, carbon, and oxygen atoms of the PPA ligand. Solvent water has been omitted for clarity.

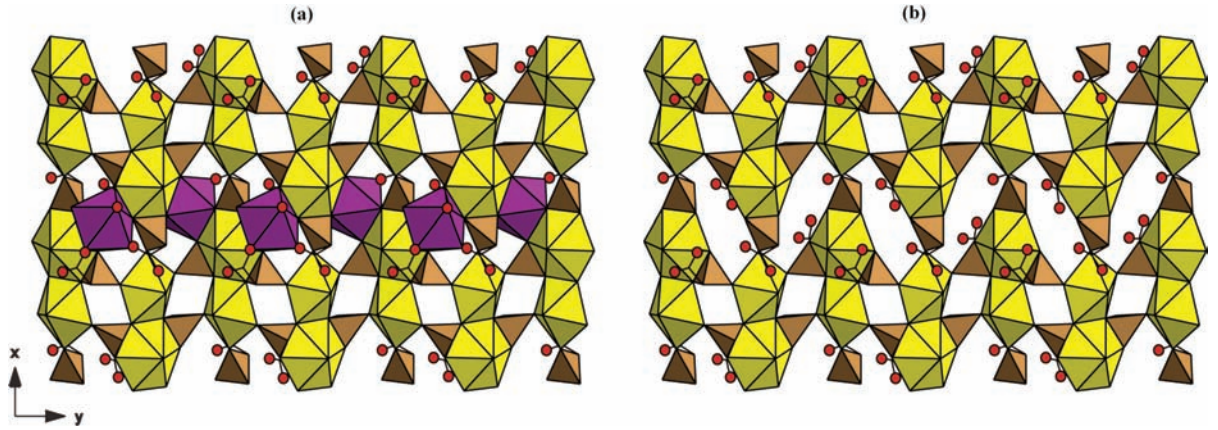

Figure 2. Polyhedral representation of the topology of the sheet (a) with and (b) without Sm^{3+} polyhedra.

measurements were fitted using *Origin 7.0*. Excitation and emission spectra were corrected for instrumental response.

RESULTS AND DISCUSSION

Structure. In previously synthesized uranium(VI)-containing carboxyphosphonates, the uranyl cation showed preferential binding to the phosphonate moiety over the carboxylate functionality.[11,13,15,16] In fact, in some of these compounds, the carboxylates were left completely uncoordinated,[11,16] opening the possibility of introducing a second metal center to coordinate to those free carboxylates.[17] The fundamental concept behind the assembly of these UO_2^{2+}-TM^{2+} materials lies in hard/soft acid/base chemistry. Where there was a hard metal cation (e.g., uranyl) and a hard functionality (e.g., phosphonate), the interaction of these was favored to the exclusion of interactions between a hard cation and a softer functionality (e.g., carboxylate). Both UO_2^{2+} and Ln^{3+} are hard metal cations, and thus the hard/soft distinction is less clear. Yet, within waste cleanup and processing chemistry, small differences in the relative stability of lanthanide and actinide complexes with a given ligand are often used to drive separations. Here, the synthesis of **1** has been achieved by harnessing the coordination preferences of the metal cations.

Compound **1** adopts a two-dimensional structure that consists of two crystallographically unique uranium metal centers, one unique samarium site, and three unique phosphonoacetate units (Figure 1). U1 is bound to two axial oxygen atoms (O1 and O2) at distances of 1.779 and 1.758 Å, respectively. U1 is then equatorially coordinated to six phosphonate oxygen atoms (O3−O8) from three phosphonoacetate ligands to form a hexagonal-bipyramid geometry. Each phosphonoacetate molecule is bound to U1 in a bidentate manner through two phosphonate oxygen atoms. U2 is similarly coordinated to two axial oxygen atoms (O10 and O11) at distances of 1.753 and 1.774 Å. U2, however, is equatorially coordinated to five phosphonate oxygen atoms from five acid units to form an overall pentagonal-bipyramid geometry; the PPA ligands are bound to U2 in a monodentate manner through $-PO_3$ oxygen atoms. Coordination of P1PA and P2PA to both U1 and U2 through phosphonate oxygen atoms O4 and O5, respectively, results in the edge-shared dimers shown in Figure 1. Further, the phosphonoacetate ligands link the dimers along [010] and [100] into the two-dimensional sheets shown in Figures 1 and 2. Additionally, there is one unique samarium metal center that is coordinated to eight oxygen atoms from four phosphonoacetate

dx.doi.org/10.1021/ic201450e | *Inorg. Chem.* 2012, 51, 201−206

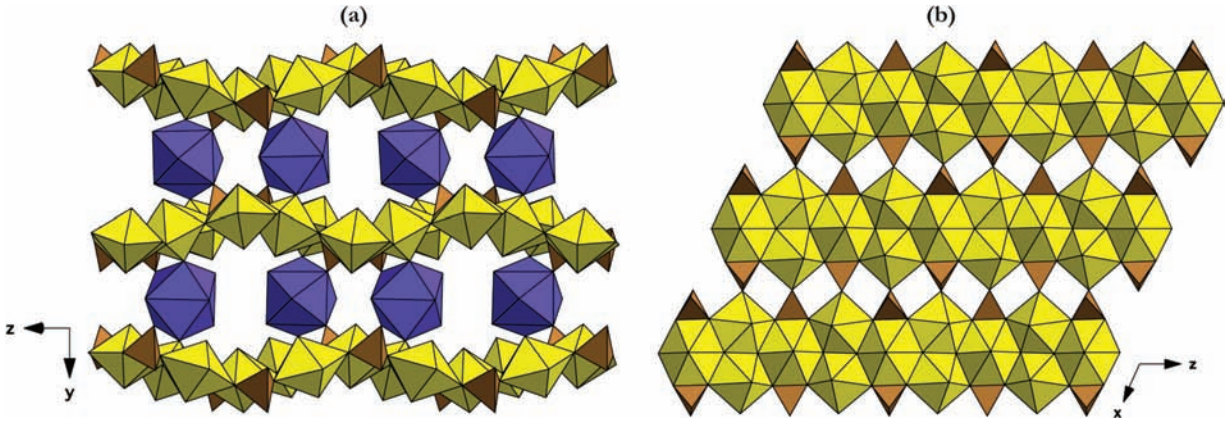

Figure 3. Polyhedral representation of francoisite (a) viewed down [100] showing the uranylphosphate sheets linked via Nd^{3+} ions and (b) illustrating the topology of the two-dimensional layers. Yellow polyhedra represent U^{VI} atoms in hexagonal- and pentagonal-bipyramid geometries. Purple polyhedra are nine-coordinate Nd^{3+} sites. Brown polyhedra represent phosphate units.

ligands and one water molecule (O18). Three of the phosphonoacetate ligands are bound to Sm^{3+} in a bidentate manner through phosphonate and carboxylate oxygen atoms, while one is bound in a monodentate manner through a single phosphonate oxygen atom (O8). Each Sm^{3+} cation edge-shares with two U1 sites through $-PO_3$ oxygen atoms O3, O8, O6, and O7. As illustrated in Figure 1, the Sm^{3+} cations essentially decorate the $[(UO_2)_2(HPPA)_2(PPA)]^{3-}$ sheets via coordination to $-CO_2$ and $-PO_3$ oxygen atoms. Finally, as shown in Figure 1b, carboxylate oxygen atoms O14, O17, and O20 are unbound and protrude into the interlayer. Solvent water is also found in the interlayer. A thermal ellipsoid plot of **1** is available in the Supporting Information (Figure S3).

Moreover, the structure of **1** may be compared to the mineral francoisite, a uranyllanthanide mineral for which the neodymium end member is of the formula $Nd[(UO_2)_3O(OH)(PO_4)_2]\cdot 6H_2O$.[50,51] Similarities include the presence of uranyl-phosphate sheets that are charge-balanced via lanthanide ions in the interlayer regions (Figure 3). In both materials, uranyl secondary building units (dimers in **1** and infinite chains in francoisite) are linked through edge-sharing phosphate groups to produce overall layered topologies. These layers are puckered in **1** with respect to francoisite, and the degree of uranyl oligomerization is much less, as can be implied from the U:P ratios (1:3 in **1** as opposed to 1:0.667 in francoisite).

Luminescence Studies. Luminescence studies show very bright visible and NIR samarium(III)-centered emission upon direct excitation of the uranyl moiety, as shown in Figure 4. The excitation spectrum (Figure S4 in the Supporting Information) shows charge-transfer bands in the range of 350−475 nm (primarily assigned to the uranyl moiety) and possibly additional weak samarium(III) f−f transitions present (see Table S1 in the Supporting Information). Because the spectrum contains multiple peaks of similar intensities, only the UO_2^{2+} excitation wavelengths (365 and 420 nm) were utilized to explore sensitization. Upon uranyl excitation, the energy is either transferred to the Sm^{3+} centers or lost to nonradiative processes within the crystal lattice. The uranyl center is nonemissive, as is evidenced by the flat region of the emission spectrum from 450 to 550 nm, where the UO_2^{2+} emission would be expected. Sm^{3+} emission is observed from 550 nm to approximately 1200 nm, with the peak assignments summarized in Table 2. For comparison, a sample of $SmCl_3$ was analyzed through excitation at 365 and 420 nm as well. Both visible and NIR emission were observed for the salt sample, albeit much less intensely, as would be expected for the direct excitation process.[52] In **1**, the Sm^{3+} emissive state exhibits a double-exponential decay with lifetimes of 67.2 ± 6.5 and 9.0 ± 1.3 μs

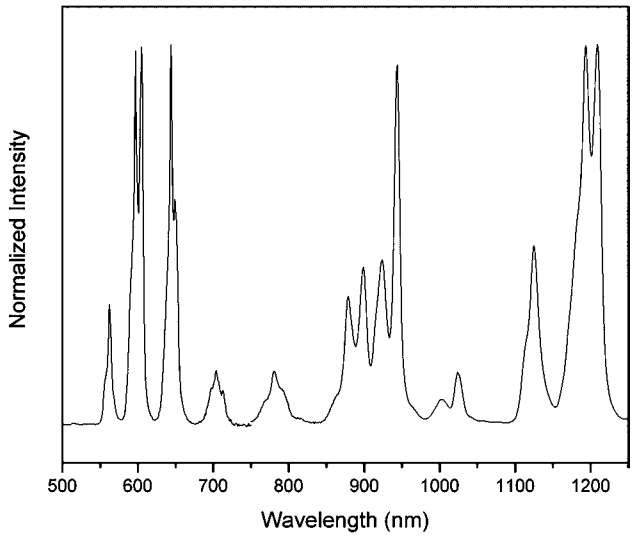

Figure 4. Visible and NIR emission from the Sm^{3+} centers upon direct uranyl excitation at 420 nm. No uranyl emission is observed between 500 and 550 nm, indicating that all energy is either transferred to the Sm^{3+} ions or lost to nonradiative pathways.

Table 2. Peak Assignment for the Observed Sm^{3+} Transitions

wavelength (nm)	transition ($^4G_{5/2} \rightarrow X$)
562	$^6H_{5/2}$
597, 605	$^6H_{7/2}$
644	$^6H_{9/2}$
703	$^6H_{11/2}$
781	$^6H_{13/2}$
879	$^4F_{1/2}$
898	$^4F_{3/2}$
923	$^6H_{15/2}$
944	$^4F_{5/2}$
1003, 1024	$^4F_{7/2}$
1125, 1194, 1209	$^6F_{9/2}$

dx.doi.org/10.1021/ic201450e | Inorg. Chem. 2012, 51, 201−206

as measured at 594 nm, after excitation at either 365 or 420 nm. The double exponential can be attributed to the different environments experienced by the Sm^{3+} ions within the crystal lattice (67 μs) and those at the surface (9 μs).[53] The larger value is within the range typically observed for Sm^{3+} emission both in the solid state and in various solvents.[54−56] These results indicate that the uranyl moiety is a highly efficient sensitizer of Sm^{3+} emission within this sample, particularly in this structure, where the U−Sm distances are quite close at approximately 4 and 6 Å. The closest uranium center is bound through bridging ligands in an edge-sharing fashion, allowing for close proximity and facilitating energy transfer.

Other lanthanide ions presented herein have emissive states higher or much lower in energy than that of the uranyl cation, making energy transfer unlikely and resulting in either UO_2^{2+} emission only or no emission at all. The U−Tb system provides an example of this. The emissive excited state of terbium(III) is located close to 20 500 cm^{-1}, and upon direct uranyl excitation, no Tb^{3+} emission and only the typical uranyl emission were observed. Lifetime measurements were conducted at 545 nm, which corresponds to a uranyl transition but also to the $Tb^{3+5}D_4 \rightarrow {}^7F_5$ transition. The observed lifetime of 25.5 ± 0.8 μs, with a single-exponential decay profile, can be attributed to the UO_2^{2+} emission, which is typically in the range of tens of microseconds,[32] while the Tb^{3+} emissive state is usually much longer lived, in the range of hundreds of microseconds to milliseconds. With a low-lying ${}^4I_{13/2}$ emissive state at approximately 6500 cm^{-1}, the U−Er system demonstrates a somewhat different energy migration pathway in that neither uranyl nor Er^{3+} NIR emission were observed, indicating the loss of any absorbed energy via nonradiative processes. The presence of uranyl emission in the terbium system and lack thereof in the erbium system indicate that energy transfer from the uranyl to the erbium is still occurring, but once the excited state of erbium is populated, the energy is lost to either lattice phonons or other deactivating vibrational modes.

CONCLUSION

We have successfully synthesized a heterometallic 4f−5f compound and characterized the uranyl sensitization of Sm^{3+}. This is an intriguing observation because previous studies of uranyl sensitization have focused on either amorphous or purely oxide phases with varying degrees of donor−acceptor concentrations. Consistent with previous studies, however, we note the appropriate match of energy levels for uranyl−Sm^{3+} energy transfer and the absence of sensitized emission in Er^{3+} and Tb^{3+} ions. Moreover, in addition to samarium luminescence, **1** shows no emission in the region typical of the uranyl cation, indicating that the energy is transferred to the Sm^{3+} center, as can be seen from the samarium-centered emission spectrum. In view of the structural diversity possible within uranyl CPs in general, one may consider the opportunity to tune (for example) Ln^{3+}−UO_2^{2+} distances and connectivity to explore the efficiency of the energy transfer as a function thereof.

ASSOCIATED CONTENT

Supporting Information

X-ray crystallographic data for complex **1** in CIF format, a thermal ellipsoid plot, powder XRD patterns of **1** and isostructural terbium, erbium, and ytterbium compounds, and luminescence data. This material is available free of charge via the Internet at http://pubs.acs.org.

AUTHOR INFORMATION

Corresponding Author

*E-mail: abd@unr.edu (A.dB.-D.), cahill@gwu.edu (C.L.C.).

ACKNOWLEDGMENTS

This material is based upon work supported as part of the Materials Science of Actinides, an Energy Frontier Research Center, funded by the U.S. Department of Energy, Office of Science, Office of Basic Energy Sciences, under Award DE-SC0001089. Support was also provided by the National Science Foundation through Grants NSF-CHE 0936982 (to D.T.d.L.) and NSF-CHE 0733458 (to A.d.B.-D.). XRD equipment was also purchased with National Science Foundation funding (Grants DMR-0348982 and DMR-0419754).

REFERENCES

(1) Renninger, N.; Knopp, R.; Nitsche, H.; Clark, D. S.; Keasling, J. D. *Appl. Environ. Microbiol.* **2004**, *70*, 7404−7412.
(2) Silva, R. J.; Nitsche, H. *Radiochim. Acta* **1995**, *70−1*, 377−396.
(3) Knopp, R.; Panak, P. J.; Wray, L. A.; Renninger, N. S.; Keasling, J. D.; Nitsche, H. *Chem.—Eur. J.* **2003**, *9*, 2812−2818.
(4) Alsobrook, A. N.; Zhan, W.; Albrecht-Schmitt, T. E. *Inorg. Chem.* **2008**, *47*, 5177−5183.
(5) Cahill, C. L.; Borkowski, L. A. U(VI)-containing metal−organic frameworks and coordination polymers. In *Structural Chemistry of Inorganic Actinide Compounds*; Krivovichev, S. V., Burns, P. C., Tananaev, I. G., Eds.; Elsevier: Amsterdam, The Netherlands, 2007; pp 409−442.
(6) Cahill, C. L.; de Lill, D. T.; Frisch, M. *CrystEngComm* **2007**, *9*, 15−26.
(7) Leciejewicz, J.; Alcock, N. W.; Kemp, T. J. *Struct. Bonding (Berlin, Germany)* **1995**, *82*, 43−84.
(8) Nelson, A.-G. D.; Albrecht-Schmitt, T. E. *C. R. Chim.* **2010**, *13*, 755−757.
(9) Thuéry, P.; Masci, B. *Cryst. Growth Des.* **2008**, *8*, 3430−3436.
(10) Thuéry, P. *CrystEngComm* **2009**, *11*, 232−234.
(11) Knope, K. E.; Cahill, C. L. *Inorg. Chem.* **2008**, *47*, 7660−7672.
(12) Knope, K. E.; Cahill, C. L. *Inorg. Chem.* **2009**, *48*, 6845−6851.
(13) Knope, K. E.; Cahill, C. L. *Inorg. Chem. Commun.* **2010**, *13*, 1040−1042.
(14) Alsobrook, A. N.; Albrecht-Schmitt, T. E. *Inorg. Chem.* **2009**, *48*, 11079−11084.
(15) Adelani, P. O.; Albrecht-Schmitt, T. E. *Inorg. Chem.* **2010**, *49*, 5701−5705.
(16) Ramaswamy, P.; Prabhu, R.; Natarajan, S. *Inorg. Chem.* **2010**, *49*, 7927−7934.
(17) Knope, K. E.; Cahill, C. L. *Eur. J. Inorg. Chem.* **2010**, *2010*, 1177−1185.
(18) Alsobrook, A. N.; Hauser, B. G.; Hupp, J. T.; Alekseev, E. V.; Depmeier, W.; Albrecht-Schmitt, T. E. *Chem. Commun.* **2010**, *46*, 9167−9169.
(19) Alsobrook, A. N.; Alekseev, E. V.; Depmeier, W.; Albrecht-Schmittt, T. E. *Cryst. Growth Des.* **2011**, *11*, 2358−2367.
(20) Alsobrook, A. N.; Hauser, B. G.; Hupp, J. T.; Aekseev, E. V.; Depmeier, W.; Albrecht-Schmitt, T. E. *Cryst. Growth Des.* **2011**, *11*, 1385−1393.
(21) Thuéry, P. *Cryst. Growth Des.* **2010**, *10*, 2061−2063.
(22) Thuéry, P. *Inorg. Chem.* **2009**, *48*, 825−827.
(23) Thuéry, P. *CrystEngComm* **2009**, *11*, 2319−2325.
(24) Thuéry, P. *CrystEngComm* **2008**, *10*, 1126−1128.
(25) Nash, K. L. *Radiochim. Acta* **1993**, *61*, 147−54.
(26) Nash, K. L. *J. Alloys Compd.* **1994**, *213-214*, 300−304.
(27) Nash, K. L. *J. Alloys Compd.* **1997**, *249*, 33−40.
(28) Nash, K. L.; Choppin, G. R. *Sep. Sci. Technol.* **1997**, *32*, 255−274.
(29) de Bettencourt-Dias, A. *Curr. Org. Chem.* **2007**, *11*, 1460−1480.
(30) Bunzli, J.-C. G. *Acc. Chem. Res.* **2006**, *39*, 53−61.

(31) Latvaa, M.; Takalob, H.; Mukkala, V.-M.; Matachescuc, C.; Rodriguez-Ubisd, J. C.; Kankarea, J. *J. Lumin.* **1997**, *75*, 149−169.
(32) Maji, S.; Viswanathan, K. S. *J. Lumin.* **2009**, *129*, 1242−1248.
(33) Lopez, M.; Birch, D. J. S. *J. Lumin.* **1997**, *71*, 221−228.
(34) Yamamura, T.; Shirasaki, K.; Sato, H.; Nakamura, Y.; Tomiyasu, H.; Satoh, I.; Shiokawa, Y. *J. Phys. Chem. C* **2007**, *111*, 18812−18820.
(35) Tanner, S. P.; Vargenas, A. R. *Inorg. Chem.* **1981**, *20*, 4384−4386.
(36) Seregina, E. A.; Seregin, A. A.; Tikhonov, G. V. *J. Alloys Compd.* **2002**, *341*, 283−287.
(37) Okamoto, Y.; Ueba, Y.; Nagata, I.; Banks, E. *Macromolecules* **1981**, *14*, 807−809.
(38) Syt'ko, V.; Bokit'ko, K. *J. Appl. Spectrosc.* **1996**, *63*, 833−840.
(39) Syt'ko, V.; Umreiko, D. *J. Appl. Spectrosc.* **1996**, *63*, 217−220.
(40) Syt'ko, V.; Umreiko, D.; Pershina, M.; Aleshkevich, N. *J. Appl. Spectrosc.* **1996**, *63*, 131−136.
(41) Joshi, B. C.; Lohani, R.; Pande, B. *J. Non-Cryst. Solids* **2004**, *337*, 97−99.
(42) Reisfeld, R.; Lieblich-Soffer, N. *J. Solid State Chem.* **1979**, *28*, 391−395.
(43) Syt'ko, V. V.; Umreiko, D. S. *J. Appl. Spectrosc.* **2001**, *68*, 377−393.
(44) Syt'ko, V.; Umreiko, D.; Aleshkevich, N.; Pershina, M. *J. Appl. Spectrosc.* **1995**, *62*, 358−362.
(45) Bruker-AXS. *APEX2*, version 3.0; Bruker Analytical X-ray Systems: Madison, WI, 2008.
(46) Sheldrick, G. *Acta Crystallogr., Sect. A: Found. Crystallogr.* **2008**, *64*, 112−122.
(47) Farrugia, L. J. *J. Appl. Crystallogr.* **1999**, *32*, 837−838.
(48) Spek, A. *J. Appl. Crystallogr.* **2003**, *36*, 7−13.
(49) Denning, R. G. *J. Phys. Chem. A* **2007**, *111*, 4125−4143.
(50) Armstrong, C. R.; Nash, K. L.; Griffiths, P. R.; Clark, S. B. *Am. Mineral.* **2011**, *96*, 417−422.
(51) Piret, P.; Deliens, M.; Piretmeunier, J. *Bull. Mineral.* **1988**, *111*, 443−449.
(52) Binnemans, K.; Görller-Walrand, C. *Chem. Phys. Lett.* **1995**, *235*, 163−174.
(53) White, K. A.; Chengelis, D. A.; Zeller, M.; Geib, S. J.; Szakos, J.; Petoud, S.; Rosi, N. L. *Chem. Commun.* **2009**, 4506−4508.
(54) Zucchi, G.; Maury, O.; Thuéry, P.; Gumy, F.; Bunzli, J. C. G.; Ephritikhine, M. *Chem.—Eur. J.* **2009**, *15*, 9686−9696.
(55) Lunstroot, K.; Nockemann, P.; Van Hecke, K.; Van Meervelt, L.; Görller-Walrand, C.; Binnemans, K.; Driesen, K. *Inorg. Chem.* **2009**, *48*, 3018−3026.
(56) Quici, S.; Cavazzini, M.; Marzanni, G.; Accorsi, G.; Armaroli, N.; Ventura, B.; Barigelletti, F. *Inorg. Chem.* **2005**, *44*, 529−537.